Nonlinear Scattering-based Imaging in Elastic Media

We 02 16

Nonlinear Scattering-based Imaging in Elastic Media

M. Ravasi* (University of Edinburgh) & A. Curtis (University of Edinburgh)

SUMMARY

Enabling nonlinear, elastic imaging using multicomponent seismic data is a key step in moving towards 'true-amplitude' imaging of the subsurface. Nonlinearity here refers both to the fact that even single-scattering interactions are in reality nonlinear (often ignored in Born-scattering migration methods), and to the nonlinearity introduced by the multiple interactions of reverberating waves with the structure to be imaged. Multiples are usually considered as noise in traditional linear imaging methods, and the nonlinearities of individual scattering events are simply ignored.

We derive two new, nonlinear elastic imaging conditions based on reciprocity theory that are suitable for reverse-time imaging of land and marine ocean-bottom data. A synthetic example shows that these outperform the best existing elastic imaging conditions, highlighting the importance of handling interactions between multiply scattered and converted waves properly. Focusing such energy in the new methods better illuminates the target and reduces imaging artifacts.

Introduction

For multicomponent recordings devices in land and marine ocean-bottom seismic acquisition, elastic reverse-time migration (Chang and McMechan, 1994) should become standard in coming years. At present, its main limitation is the interference of kinematically independent wave modes propagating in an elastic media. Yan and Sava (2008) suggest an imaging condition (IC) that crosscorrelate P- and S-waves separated in the subsurface after vector wavefield extrapolation. This algorithm has shown some promise because it results in elastic images with better focusing than their acoustic counterpart (Lu et al., 2009). However, their IC assumes only single, linear scattering from perturbations to the medium.

In this paper we generalize that procedure and formulate new nonlinear, elastic ICs based on reciprocity (Wapenaar and Fokkema, 2006) which account for multiply scattered and multiply converted waves, properly focusing such energy at each image point. Resulting images show more details and fewer artifacts than when using the previous imaging condition.

Theory of nonlinear elastic imaging conditions

A seismic image can be defined as a zero-offset, zero-time, scattered wavefield evaluated at every image point in the subsurface (e.g., Claerbout, 1971; Vasconcelos et al., 2010). Thus, when elastic imaging is accomplished, pure- or converted-mode elastic images represent a scattered P- or S-wave virtually recorded at every image point $\mathbf{x}$ due to a colocated P- or S-wave virtual source (Figure 1)

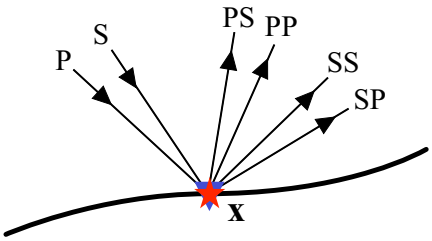

Figure 1 *A sketch depicting an elastic imaging condition based on the concept of a zero-offset, zero-time scattered wavefield. A P- or S-wave virtual source (red star) is fired at any image point* $\mathbf{x}$ *and the local wavefield is recorded by a colocated P- or S-wave virtual receiver (blue triangle).*

Given an elastic correlation-type representation theorem in the frequency domain (Wapenaar and Fokkema, 2006 - eq. 63), we express any involved Green's function as the sum of a reference and scattered components ($G = G^0 + G^S$), and in terms of P- or S-wave virtual receivers colocated at $\mathbf{x}$ (i.e., zero-offset response). Integrating over frequencies (ω) to get the zero-time response, we obtain

$$I_{NI}^{nonlinear}(\mathbf{x}) = G_{(I,N)}^{S(\Phi,\Phi)}(\mathbf{x},\mathbf{x},\tau=0) = -\int_0^{+\infty}\int_{\partial V_S}\left(\bar{G}_{(I,ij)}^{S(\Phi,h)}(\mathbf{x},\mathbf{x}_S)\left\{G_{(N,i)}^{0(\Phi,f)}(\mathbf{x},\mathbf{x}_S)\right\}^* + \bar{G}_{(I,i)}^{S(\Phi,f)}(\mathbf{x},\mathbf{x}_S)\left\{G_{(N,ij)}^{0(\Phi,h)}(\mathbf{x},\mathbf{x}_S)\right\}^*\right) n_{S_j}\, d\mathbf{x}_S\, d\omega$$
$$-\int_0^{+\infty}\int_{\partial V_S}\left(\bar{G}_{(I,ij)}^{(\Phi,h)}(\mathbf{x},\mathbf{x}_S)\left\{G_{(N,i)}^{S(\Phi,f)}(\mathbf{x},\mathbf{x}_S)\right\}^* + \bar{G}_{(I,i)}^{(\Phi,f)}(\mathbf{x},\mathbf{x}_S)\left\{G_{(N,ij)}^{S(\Phi,h)}(\mathbf{x},\mathbf{x}_S)\right\}^*\right) n_{S_j}\, d\mathbf{x}_S\, d\omega \quad (1)$$

where terms $G_{(N,i/ij)}^{0(\Phi,f/h)}(\mathbf{x},\mathbf{x}_S) / G_{(N,i/ij)}^{S(\Phi,f/h)}(\mathbf{x},\mathbf{x}_S)$ are the reference/scattered source wavefields (i.e., directly modelled) and $\bar{G}_{(I,i/ij)}^{S(\Phi,f/h)}(\mathbf{x},\mathbf{x}_S) / \bar{G}_{(I,i/ij)}^{(\Phi,f/h)}(\mathbf{x},\mathbf{x}_S)$ are the scattered/total receiver wavefields (i.e., backpropagated from recorded data). Superscripts between brackets represent the observed quantity (Φ: potentials) and the source quantity (f: external volume force, h: external deformation rate), while subscripts identify the components of the observed quantity and the source quantity, $\mathbf{x}_S$ spans locations of physical sources, n_{S_j} is the *j*-th component of the normal vector on the (ideally, closed) boundary of sources ∂V_S, and the superscript * denotes complex conjugation.

Equation (1) can be regarded as a nonlinear, 'true-amplitude' (under ideal acquisition geometries) IC suitable for land seismic acquisition, where the second line allows for proper mapping of nonlinear interactions (Fleury and Vasconcelos, 2012) in the subsurface.

Since the formulation with force and deformation sources is not practical for marine ocean-bottom applications, we change source quantities to be P-wave sources, assuming that the medium at, and outside of ∂V_S is homogeneous, isotropic and unperturbed. A second nonlinear, 'true-amplitude' IC, suitable for marine ocean-bottom seismic acquisition is thus derived

$$I_{NI}^{nonlinear}(\mathbf{x}) \approx \frac{2}{\rho c_0}\int_0^{+\infty}\int_{\partial V_S}\left[G_{(N,P)}^{0(\Phi,\Phi)*}(\mathbf{x},\mathbf{x}_S)\bar{G}_{(I,P)}^{S(\Phi,\Phi)}(\mathbf{x},\mathbf{x}_S)+G_{(N,P)}^{S(\Phi,\Phi)*}(\mathbf{x},\mathbf{x}_S)\bar{G}_{(I,P)}^{(\Phi,\Phi)}(\mathbf{x},\mathbf{x}_S)\right]d\mathbf{x}_S\,d\omega \qquad (2)$$

In the context of traditional elastic imaging, where discontinuities are mapped in the subsurface using only primary reflections (i.e., assuming Born-like scattering), equation (2) is simplified and nonlinear terms are neglected,

$$I_{NI}^{linear}(\mathbf{x}) \approx \frac{2}{\rho c_0}\int_0^{+\infty}\int_{\partial V_S} G_{(N,P)}^{0(\Phi,\Phi)*}(\mathbf{x},\mathbf{x}_S)\bar{G}_{(I,P)}^{S(\Phi,\Phi)}(\mathbf{x},\mathbf{x}_S)d\mathbf{x}_S\,d\omega \qquad (3)$$

This is exactly the IC proposed by Yan and Sava (2008), apart from the $2/\rho c_0$ scaling. They create a seismic image by crosscorrelating the source wavefield and the receiver wavefields, depth extrapolated by solving numerically a boundary-value problem for the elastic wave-equation, where the boundary condition consists of the wavefield recorded on the Earth's surface. Wavefield separation into scalar and vector potentials is carried out in the subsurface at each image point, then the imaging condition is applied.

Example

A simple synthetic example is used to compare our nonlinear IC (equation (2)) and the linear IC (equation (3)). An isotropic homogeneous medium is used as the background (reference) medium, and a high-velocity square that contains a point scatterer at its center represents the perturbation to be imaged (Figure 2). P-wave physical sources are distributed along a circular boundary with radius $r = 0.4\ km$ to illuminate the target.

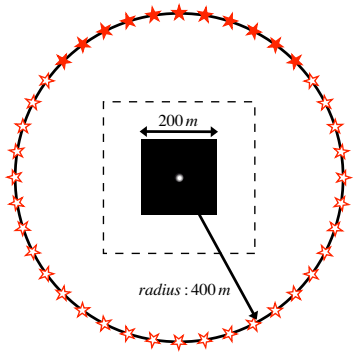

Figure 2 *Geometry used for the imaging example. The image has been created inside the dashed lines using a circular boundary of 40 P-wave sources. The sides and bottom sources (open stars) are active when the illumination is complete, and inactive when the illumination is partial, while the top sources (solid stars) are always active. The P-wave velocity of the background medium is* $v_P = 1.5\ km/s$, *the square represents a strong positive perturbation of* $\Delta v_P = 1.3\ km/s$, *and the point scatterer S represents a negative perturbation of* $\Delta v_P = -1.2\ km/s$ *with respect to the latter. S-wave velocity is a scaled version of P-wave velocity, with* $v_P / v_S = 2$.

Source and receiver wavefields are computed using a 2D elastic finite-difference algorithm. We use an exact, noiseless receiver wavefield at each image point $\mathbf{x}$ rather than an approximated version coming from wavefield extrapolation in order to compare the effectiveness of different ICs without additional confounding sources of extrapolation error. Note that, since only P-wave sources are used (as in marine seismic) and the reference medium is homogenous, the S-wave component of the reference source wavefield is always zero. Hence, we compare the images produced by crosscorrelating the P-wave components of the source wavefield with the P- and S-wave components of the receiver wavefield (I_{PP}, I_{PS}). We interpret the additional contribution of the interaction between scattered wavefields and we analyze the effect of illumination on these images by considering complete illumination (all sources active) and partial illumination (only top sources are active - Figure 2).

In the ideal imaging experiment, PP linear imaging (Figure 3a) recovers only the square object; strong transmission artifacts (i.e., artifacts due to the interactions between the reference wavefield and forward-scattered waves that traverse the square object) contaminate the image preventing a clear

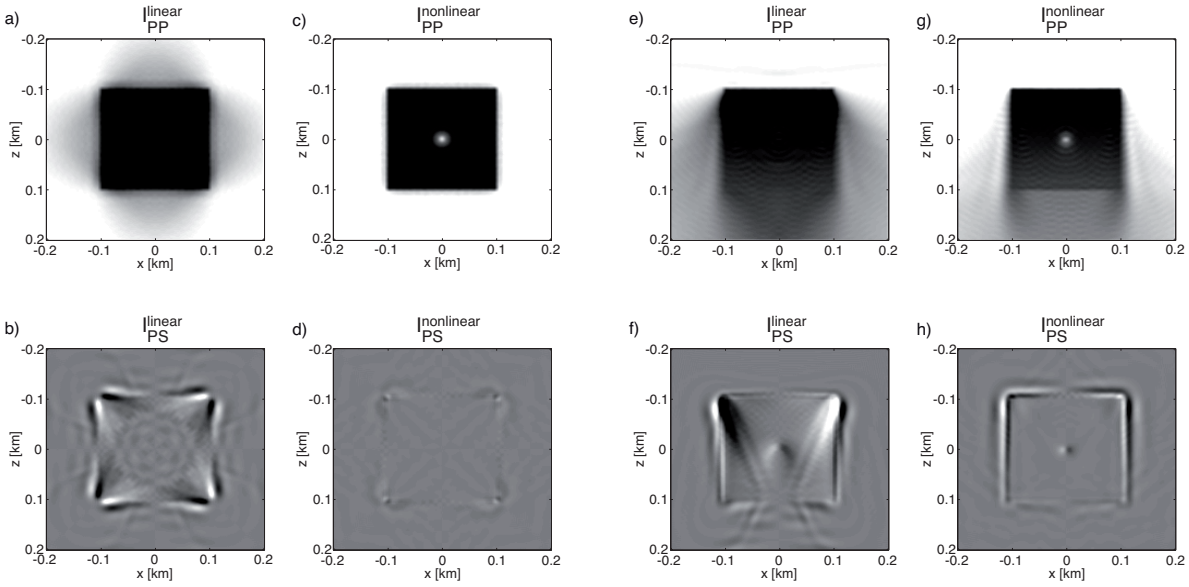

Figure 3 *PP and PS images using complete and partial boundary of physical sources produced with a linear imaging condition (a,b,e,f) that crosscorrelates P- and S-wave potentials separated in the subsurface after a vector wavefield extrapolation (Yan and Sava, 2008), and our nonlinear imaging condition (c,d,g,h). Images (a) and (c) are* I_{PP}*, while (b) and (d) are* I_{PS} *with complete source boundary illumination. Images (e) and (g) are* I_{PP}*, while (f) and (e) are* I_{PS} *with partial boundary illumination.*

definition of its shape. A proper mapping of nonlinear contributions (i.e., multiply scattered and multiply converted waves) is the key to achieve exact imaging, where scattering objects are constructed at correct locations with correct amplitudes. The square perturbation with the point scatterer at its center is correctly imaged using the nonlinear IC in equation (2) (Figure 3c).

Linear PS imaging (Figure 3b) outlines the edges of the square with a polarity change between left and right sides (most obvious on the horizontal edges of the square). More strikingly, the nonlinear interaction between converted scattered waves perfectly matches the contributions of linear interactions between reference and scattered waves and results in a final image that is almost perfectly null (Figure 3d), with the exception of some weak artifacts around the corners of the square. An intuitive explanation comes from the fact that the sign of the reflection coefficient of a converted wave is a function of the P-wave incidence angle (Balch and Erdemir, 1994). Thus, when PS images with flipped polarities are stacked over all the shots, destructive interference occurs. However, this result is also consistent with our earlier definition of an imaging condition: the impossibility to create a zero-time conversion from a zero-offset experiment explains why the image is completely null (when the estimate of the total source power loss is accurate at every point, thanks to having complete illumination - in contrast to results below).

When imaging is accomplished with a partial boundary of sources, artifacts arise on both sides of and below the square in the linear PP image (Figure 3e and f). Although having an incomplete illumination breaks the power conservation (Fleury and Vasconcelos, 2012), nonlinear imaging is still more accurate and the additional contribution of the interaction between scattered wavefields partially removes the artifacts, especially those on vertical sides of the square, and also identifies the point scatterer at its center (Figure 3g). Imaging of PS converted waves with an uneven illumination creates a partial set of images that, when stacked together, do not perfectly cancel each other leaving some residual artifacts in the final image (Figure 3f). Nonlinear interactions play a role in the attenuation of such spurious energy, even if they can not completely compensate for the absence of bottom sources below the medium (Figure 3h).

We conclude that even if the zero-time scattered wave response generated by zero-offset pseudo-experiments is a good candidate for imaging of pure-mode elastic waves, it may not be the best condition for imaging of converted-mode elastic waves. Every attempt to reduce or remove the destructive summation by correcting the polarity of converted waves (e.g., by sign flips - Figure 4) can now be seen as an attempt to obtain an image that does *not* resemble the zero-time, scattered-wave response generated by zero-offset pseudo-experiments. We conjecture that a more appropriate context for elastic imaging of converted waves is represented by extended images (Sava and Vasconcelos, 2010) where imaging conditions at non-zero subsurface offset are used (Halliday and Curtis, 2010).

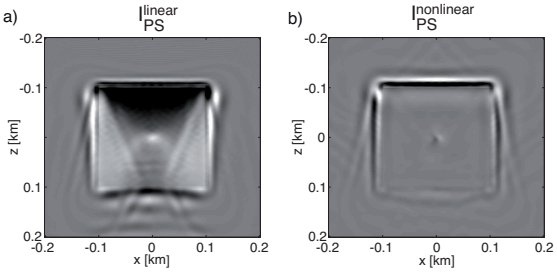

Figure 4 *PS images with only the partial illumination in Figure 2 when polarity correction is applied before stacking for (a) linear and (b) nonlinear imaging. Nonlinear terms still contribute to reduce artifacts around the interfaces, and to sharpen up the entire image.*

Conclusions

A correlation-type representation theorem for perturbed elastic media with P- or S-wave colocated virtual receivers in the subsurface is used to formulate two new nonlinear, 'true-amplitude' elastic ICs. They can be interpreted as theoretically exact versions of a previous, heuristically-derived IC that crosscorrelates pure- or converted-modes separated in the subsurface after a vector wavefield extrapolation. This result creates an explicit link between the theory of reciprocity and elastic seismic imaging, and sheds new light on how to create true-amplitude elastic images.

Acknowledgements

The authors are grateful to Ivan Vasconcelos (Schlumberger Cambridge Research) and Giovanni Angelo Meles (University of Edinburgh) for insightful discussions. We also thank the Edinburgh Interferometry Project (EIP) sponsors for supporting this research and granting us permission to publish it.

References

Balch, A. and Erdemir C. [1994] Sign-change correction for prestack migration of P-S converted wave reflections. Geophysical Prospecting, **42**, 637–663.

Chang, W.-F. and McMechan, G. A. [1994] 3-D elastic prestack, reverse-time depth migration. Geophysics, **59**, no. 4, 597–609.

Claerbout, J. F. [1971] Toward a unified theory of reflector mapping. Geophysics, **36**, no. 3, 467-481.

Fleury, C. and Vasconcelos, I. [2012] Imaging condition for nonlinear scattering-based imaging: Estimate of power loss in scattering. Geophysics, **77**, no. 1, S1-S18.

Halliday, D., and A. Curtis, [2010] An interferometric theory of source-receiver scattering and imaging. Geophysics, **75**, SA95–SA103.

Lu, R., Traynin, P. and Anderson, J. E. [2009] Comparison of elastic and acoustic reverse time migration on the synthetic elastic marmousi-ii obc dataset. 79th Annual International Meeting, SEG, Expanded Abstracts.

Sava, P. and Vasconcelos, I. [2010] Extended imaging condition for wave-equation migration. Geophysical Prospecting, **59**, 35-55.

Vasconcelos, I., Sava, P. and Douma, H. [2010] Nonlinear extended images via image-domain interferometry. Geophysics, **75**, SA105-SA115.

Wapenaar, K. and Fokkema, J. [2006] Green's function representations for seismic interferometry. Geophysics, **71**, SI33–SI46.

Yan, J. and Sava, P. [2008] Isotropic angle-domain elastic reverse-time migration. Geophysics, **73**, S229–S239.